HHS Public Access

Author manuscript

Acta Biomater. Author manuscript; available in PMC 2020 April 15.

Published in final edited form as:

Acta Biomater. 2019 April 15; 89: 84–94. doi:10.1016/j.actbio.2019.03.025.

Elucidating the Role of Graft Compliance Mismatch on Intimal Hyperplasia using an Ex Vivo Organ Culture Model

Allison Post[#1], **Patricia Diaz-Rodriguez**[#2], **Bailey Balouch**[2], **Samantha Paulsen**[3], **Siliang Wu**[4], **Jordan Miller**[3], **Mariah Hahn**[2,*], and **Elizabeth Cosgriff-Hernandez**[4,*]

[1]Department of Biomedical Engineering, Texas A&M University, College Station, Texas, 77843

[2]Department of Biomedical Engineering, Rensselaer Polytechnic Institute, Troy, New York 1218

[3]Department of Biomedical Engineering, Rice University, Houston, Texas 77005

[4]Department of Biomedical Engineering, University of Texas, Austin, Texas, 78712

[#] These authors contributed equally to this work.

Abstract

There is a growing clinical need to address high failure rates of small diameter (< 6 mm) synthetic vascular grafts. Although there is a strong empirical correlation between low patency rates and low compliance of synthetic grafts, the mechanism by which compliance mismatch leads to intimal hyperplasia is poorly understood. To elucidate this relationship, synthetic vascular grafts were fabricated that varied compliance independent of other graft variables. A computational model was then used to estimate changes in fluid flow and wall shear stress as a function of graft compliance. The effect of compliance on arterial remodeling in an *ex vivo* organ culture model was then examined to identify early markers of intimal hyperplasia. The computational model prediction of low wall shear stress of low compliance grafts and clinical control correlated well with alterations in arterial smooth muscle cell marker, extracellular matrix, and inflammatory marker staining patterns at the distal anastomoses. Conversely, high compliance grafts displayed minimal changes in fluid flow and arterial remodeling, similar to the sham control. Overall, this work supports the intrinsic link between compliance mismatch and intimal hyperplasia and highlights the utility of this *ex vivo* organ culture model for rapid screening of small diameter vascular grafts.

Keywords

Vascular graft; compliance; intimal hyperplasia; bioreactor; computational model; wall shear stress

[*]Co-corresponding Authors. Corresponding author address: 107 W. Dean Keaton, BME 3.503D, 1 University Station, C0800, Austin, TX 78712, Tel: (512) 471-7679.

1. INTRODUCTION

Coronary artery bypass grafting procedures are one of the most commonly performed surgeries in the United States today, with 397,000 performed every year [1]. Typically, autologous grafts from the saphenous vein or mammary artery are used; however, these autografts are not available in up to 20% of patients due to disease, size mismatch, or the need for multiple grafts (e.g. quintuple bypass procedures) [1]. Synthetic vascular grafts composed of expanded polytetrafluoroethylene (e.g. Gore-tex®) or polyethylene terephthalate (e.g. Dacron®) have demonstrated satisfactory long-term outcomes in large- (>8 mm) and medium-diameter (6 - 8 mm) arteries, but poor patency limits their application in small-diameter vessels (< 6mm) and has been attributed to thrombosis and the development of intimal hyperplasia [2]. Intimal hyperplasia causes failure of approximately 10-30% of synthetic grafts [3, 4]. This high rate of failure has been correlated with a compliance mismatch between the grafting material and the native vasculature, in which compliance is a measure of the change in vessel diameter over a change in pressure [3, 5]. Despite this strong empirical correlation, the mechanisms by which compliance mismatch leads to intimal hyperplasia are relatively poorly understood. It is theorized that the compliance mismatch leads to a flow disruption at the distal anastomosis, which then leads to low wall shear stress [3, 6]. The vessel wall, in response to the low wall shear stress, attempts to correct the flow disruption with intimal thickening, ultimately leading to re-occlusion of the vessel [5]. In order to design vascular grafts with improved patency, the complex cascade of events that begins with changes in the endothelium and initiates the smooth muscle cell phenotypic alterations that typify intimal hyperplasia need to be elucidated.

It has been difficult to directly relate compliance-mismatch and the resulting changes in fluid dynamics to the development of intimal hyperplasia because of confounding factors of graft properties. For example, the often cited high-compliance grafts with improved patency are autografts as compared to the low-compliance synthetic grafts [5]. Isolation of the effect of compliance is ideally conducted on synthetic grafts that can vary compliance independent of other graft variables. We have previously reported on the fabrication of multi-layer vascular grafts with tunable biomechanical properties and improve compliance matching that enables this investigation [7, 8]. In addition, to elucidate the role of compliance on the change in blood flow, a quantitative prediction of the change in wall shear stress as a function of graft compliance is needed. Computational models have been used to predict changes in blood flow and wall shear stress in stenting of coronary arteries to improve the design iteration process for vascular stents [9–11]. In this study, we propose to use a simple computational model of the synthetic graft-artery anastomosis to provide a prediction of wall shear stress as a function of graft compliance that can be directly correlated to changes observed in distal arterial remodeling. Finally, evaluation of vascular grafts includes assessment of long-term patency and incidence of intimal hyperplasia using large animal models that can be both time and cost-prohibitive [12]. A method to rapidly screen vascular grafts for early markers of intimal hyperplasia using an *ex vivo* organ culture model would enhance vascular graft development.

To this end, the established changes in the vessel wall composition and structure during intimal hyperplasia were reviewed to identify early markers that can be used to screen candidate grafts in an *ex vivo* organ culture model. Central to the disease progression are the changes to vascular smooth muscle cells (VSMCs). VSMCs are highly specialized cells responsible for the contraction and regulation of blood vessel tone, blood pressure, and blood flow [13]. In normal adult arteries, differentiated VSMCs present low proliferation rates and exhibit a contractile phenotype expressing proteins such as smooth muscle myosin heavy chain (SM-MHC), smooth muscle α-actin (SMα-actin), smooth muscle 22α (SM22α), and calponin hi, important for the regulation of the vessel contraction [13–15]. When intimal hyperplasia is initiated due to trauma, changes in wall shear stress, or inflammation, VSMCs undergo a de-differentiation process towards a proliferative phenotype, These proliferative VSMCs display altered expression of contractile proteins (ie. maintained/increased expression of early contractile markers SMa-actin and SM22α and decreased expression of later-term contractile markers) and of the cell-cell adhesion molecule N-Cadherin. These changes are associated with increased VSMC migration towards the innermost layer of the arterial wall and arterial wall thickening [16–18]. Proliferative VSMCs also present higher expression of interstitial matrix components (e.g. versican, elastin, and fibronectin) [14, 15, 19, 20] and increased expression of matrix metalloproteinases (e.g. MMP-1, MMP-2, and MMP-9) [13, 15, 19].

Although most of the intimal hyperplasia morphological changes are associated with the phenotypic switch of VSMCs, all the components of the vessel play an important role in the modulation of the disease initiation and progression [20]. Vascular endothelial cells are key regulators of vessel homeostasis and secrete molecules able to prevent coagulation, promote vasodilation, and control VSMCs proliferation and differentiation [19, 20]. However, in the presence of abnormal laminar blood flow or injury, endothelial cells become dysfunctional and secrete agents that promote coagulation and vasoconstriction, switch VSMCs to a proliferative phenotype, and stimulate the infiltration of inflammatory cells. Dysfunctional endothelial cells display altered levels of the adherens junction molecule VE-Cadherin, critical to regulating endothelium permeability, as well as increased expression of N-Cadherin, which mediates heterotypic contacts with VSMCs [21–23]. Furthermore, abnormally stimulated endothelial cells produce altered levels of cytokines (e.g. PDGF, TGF-β1, IL-6, and TNF-α) that further stimulate VSMC-based ECM remodeling [19, 24] as well as display increased expression of pro-inflammatory markers such as van Willebrand Factor (vWF), E-selectin, and P-selectin [19].

In the current study, an *ex vivo* organ culture model was developed to analyze the histological changes in grafted porcine carotid arteries in response to an increased compliance matching of the grafts. First, grafts of distinct compliances were fabricated and compliance was evaluated before suturing to the carotid arteries and culturing in the *ex vivo* bioreactor [7]. The distal anastomoses were analyzed after two weeks of culture for changes in VSMC phenotype (SM22α, SMα-actin, N-Cadherin, and proliferation marker Ki67), the endothelium (VE-Cadherin, vWF, N-Cadherin), and extracellular matrix composition (versican, elastin, fibronectin), as early markers of intimal hyperplasia. Finally, these findings were correlated to a predictive computational model of wall shear stress in a grafted carotid artery with increasing compliance of the graft. This study elucidates not only the

intrinsic link between graft compliance mismatch and the development of intimal hyperplasia, it also provides a screening method for synthetic small diameter vascular graft development.

2. MATERIALS AND METHODS

2.1 PEGDAA synthesis

Polyethylene glycol diacrylamide (PEGDAA) was synthesized according to a method adapted from Hahn, et al [25]. Briefly, acryloyl chloride (4 molar equivalents) was added dropwise to a solution of PEG diamine (3.4 kDa; 1 molar equivalent) and triethylamine (TEA, 2 molar equivalents) in anhydrous dichloromethane (DCM) under nitrogen. The reaction was stirred for 24 hours, and then washed with 2M potassium bicarbonate (8 molar equivalents). After drying with anhydrous sodium sulfate, the product was precipitated in cold diethyl ether, vacuum filtered, and dried under vacuum.

2.2 Multilayer graft fabrication

A 25 wt% solution of Bionate® segmented polyurethane (DSM Biomedical) in dimethylacetamide was electrospun with a flow rate of 0.5 ml/hr through a blunted 20G needle. The rotating mandrel for collection was first coated in a PEG sacrificial layer and placed 50 cm from the needle tip. A voltage of 15 kV was applied to the needle and a −5kV voltage was applied to the rotating mandrel (rotational speed of 5000 rpm). To generate grafts of varying compliance, mesh thickness was varied from 0.1–0.4 mm by adjusting collection time with increasing thickness resulting in reduced graft compliance. [8] The rod and mesh were allowed to soak for 1 hour in water to dissolve out the sacrificial PEG layer, and the mesh sleeve was cut into 4 mm long sections. Fiber diameter and mesh thickness was examined using scanning electron microscopy (SEM; Phenom Pro, NanoScience Instruments, Phoenix, AZ) at 10 kV accelerating voltage. Prior to imaging, the specimens were coated with 4 nm of gold using a sputter coater (Sputter Coater 108, Cressington Scientific Instruments, Hertfordshire, UK). Average fiber diameter was determined by drawing a horizontal line through the SEM images of the graft meshes and measuring the diameter of the first ten fibers crossed by the line using ImageJ software. Three images per selected graft were analyzed for a total of n = 30 fibers per group. For composite fabrication, electrospun mesh sleeves were then taken through a graded ethanol/water soak (70%, 50%, 30%, and 0%; 30 minutes each) to ensure hydration and penetration of the aqueous hydrogel precursor solutions into the mesh prior to hydrogel coating. The pre-wetted meshes were then placed in a cylindrical mold with an inner glass mandrel (4 mm outer diameter to match the vessel inner diameter). The hydrogel precursor solution (7.2% PEGDAA, 3.6% n-vinyl pyrrolidone (NVP), and 1% Irgacure solution) was pipetted between the mandrel and the hydrated mesh and photocrosslinked with UV light for 6 minutes in a custom-built UV box. This method results in composite grafts with a constant inner diameter of 4 mm inner diameter regardless of electrospun mesh thickness. Uniform matching of the vessel inner diameter is an important consideration to limit confounding variables when assessing fluid-material interactions at the graft-vessel anastomosis. The hydrogel layer thickness varies accordingly but we have demonstrated that the hydrogel does not contribute significantly to the compliance or burst pressure properties of the composite graft (Supplementary Figure 1).

Composite grafts were then soaked for three days in distilled water with daily solution changes to remove un-reacted NVP. The grafts were then trimmed to approximately 4 cm in length for biomechanical analysis and 2 cm in length for the bioreactor studies.

2.3 Computational modeling

A computational fluid dynamics model was used to assess changes in wall shear stress as a function of graft compliance. Simulations were developed using COMSOL Multiphysics 5.3, the Computational Fluid Dynamics (CFD) physics module and solving all models under steady-state conditions. All models were assumed to be in the laminar flow regime, with Reynolds numbers on the order of 1000. The 3D geometry of the graft was simulated using an axially symmetric model, where a detailed schematic of the model geometry is shown in Figure 2. The vessel segments on either end of the graft were 10 cm long with 4 mm inner diameter and the far ends of these vessels (the ends not attached to the graft segment) were modeled as a fixed boundary condition. The inner diameter of the vessels at 80 mmHg and 120 mmHg was determined experimentally from laser micrometer measurements of arterial segments of compliance of 9.0 %/mm Hg × 10^{-2} measured at these pressures. The central graft region was 4 cm long with 4 mm inner diameter. The differences in inner diameter as a function of graft compliance was measured experimentally as described above and inputted into separate models of grafts to model compliance 1.5, 4.0, and 8.5 %/mm Hg × 10^{-2}. Blood flow was modeled using the Carreau Yasuda model of blood viscosity:

$$\mu = \mu_{\infty} + (\mu_0 - \mu_{\infty})[1 + (\lambda\dot{\gamma})^2]^{(n-1)/2}$$

where

$$\lambda = 3.313s$$

$$n = 0.3568$$

$$\mu_0 = 0.56P$$

$$\mu_{\infty} = 0.0345P$$

that have been previously used for blood flow modeling [26, 27], and fluid-contacting walls within the geometry were modeled with a no-slip boundary condition. A relative pressure drop of 40 mmHg was modeled to mimic a physiological pressure drop from 120 mmHg to 80 mmHg by setting inlet pressure to 40 mmHg and an outlet pressure to 0 mmHg. Fluid flow through the fixed inlet was set to physiological parameters at 395 ml/min. This value corresponds to the average flow rate within the common carotid artery. [28] Wall shear stress was then calculated using the formula below:

$$\tau = \mu\left(\frac{du}{dy} + \frac{dv}{dx}\right)$$

where *du/dy* is the streamwise velocity and *dv/dx* is the spanwise velocity. The mesh for computation included corner refinements to ensure solution accuracy with a minimum angle between boundaries of 240° and element size scaling factor 0.25. 144,682 mesh elements make up the model, with the lowest mesh quality at 0.4, and the overall average mesh quality of 0.8, well beyond the typical 0.1 mesh quality limit. A mesh analysis was performed to confirm model convergence (Supplementary Figure 2).

2.4 Ex vivo arterial culture

Carotid arteries sutured to grafts of varying compliance were cultured in a novel *ex vivo* bioreactor system under physiological conditions to correlate compliance mismatch to arterial remodeling (Figure 3A**)**. Fresh porcine carotid arteries were purchased from LAMPIRE Biological Laboratories, Inc. (Pipersville, PA). Arteries were dissected in a laminar flow hood to remove excess of connective tissue and rinsed multiple times with PBS containing antibiotics and antimycotics (PBS-PSA, Gibco). Arteries were then sectioned into three pieces and distributed as follows: three 2 cm long pieces and a central 2 mm long piece were harvested. The central 2 mm piece was formalin-fixed and was used to assess initial “day 0” arterial morphology and protein expression. The two outermost 2 cm segments were anastomosed using a 7-0 prolene surgical needle (Ethicon) to different grafts: 1) multilayer grafts of low compliance, 2) multilayer grafts of medium compliance, 3) multilayer grafts of high compliance, 4) expanded poly(tetrafluoroethylene) (ePTFE) graft positive controls (GORE-TEX® Stretch Vascular Graft ST04015A) or 5) the central 2 cm arterial segments (negative controls). The anastomoses of the grafted vessels were then sealed using surgical glue (Coseal, Baxter), rinsed with PBS-PSA to check for flow and leaking, and mounted within a bioreactor chamber (BISS Tissue Growth Technologies) (Figure 3B,C). The vessels were then fixed into place using a sterile nylon thread.

The bioreactor system was then washed with PBS-PSA prior to the onset of flow to confirm absence of leakages. Complete Endothelial Growth Medium (EGM; DMEM supplemented with 20% bovine calf serum (BCS), 2% PSA, EGF, bFGF, VEGF, long R3 IGF1, ascorbic acid, heparin and hydrocortisone) was placed inside the artery chambers while the lumen of the grafted vessels was perfused with EGM supplemented with 35 mg/ml of pharmaceutical grade Dextran (Dextran T70, Pharmacosmos) as a thickening agent. Flow through the grafts was generated using a peristaltic pump (Masterflex L/S 07528-30) at a rate of 30 ml/min, similar to that utilized in previous *ex vivo* carotid artery bioreactor studies.[29, 30] The peristaltic pump resulted in a pulsatile waveform, and pressure in the system was adjusted to achieve ~120 mmHg/80 mmHg peak-to-trough pressures. Four independent bioreactor studies were performed for each experimental formulation.

After 14 days of culture, arterial segments at distal anastomosis of each grafted vessel were then harvested (Figure 3C), embedded in optimal cutting temperature compound (OCT) and cryosectioned at 5 μm thickness. Cryosections at 1.2-1.7 mm from the distal graft-host anastomosis were utilized for immunohistochemical analysis, with at least two independent

immunostainings performed. Cell number and viability throughout 14 day culture period was first evaluated and confirmed by sustained levels of DAPI nuclear staining in each construct relative to day 0 (Supplementary Figure 3). Representative images of “day 0” vessels are provided in Supplementary Figure 4.

2.5 Immunohistochemistry and autofluorescence-based elastic fiber assessment

Alterations in VSMC phenotype, endothelial cell phenotype, and extracellular matrix proteins were analyzed using standard immunohistochemical technique. Cryosections that were between 1.2-1.7 mm from the distal graft-host anastomosis were rehydrated at room temperature for 15 min, then endogenous peroxidases were blocked for 10 min, followed by 10 min exposure to Terminator solution (BioCare Medical) to block nonspecific background staining. Sections were then incubated with the appropriate primary antibody for 1 h at room temperature (Supplementary Table 1). The binding of the primary antibody was detected by incubating the samples with HRP-conjugated secondary antibodies (Jackson ImmunoResearch) for 1 h at room temperature followed by the application of the DAB chromogen (Vector Laboratories). Stained sections were imaged using a Zeiss Axiovert microscope. For each independent bioreactor run, at least two cryosections were immunostained and analyzed for each treatment group. Furthermore, elastic fiber density and structure was assessed by harnessing the autofluorescence of elastic fibers and imaging rehydrated cryosections (2 per treatment group per bioreactor run) using FITC filters.

2.5.1 Semi-quantitative assessment of immunostaining—For each immunostained arterial cryosection, a series of brightfield images were obtained using a Zeiss Axiovert microscope. Whole artery images were subsequently generated from the image series using the “mosaic” function within Photoshop software. For each antibody utilized to characterize VSMC function or medial layer ECM, the assembled mosaic images were then FITC filters. analyzed to semi-quantitatively evaluate overall staining intensity and staining distribution per standard techniques. In brief, overall staining intensity of each VSMC or ECM antibody for a particular graft type within each reactor experiment was evaluated on a scale of 0-3, with 0 representing no staining and 3 representing the highest staining intensity for that antibody within that reactor experiment. Following quantification of each graft formulation within each of the four reactor experiments, average staining intensity for a given graft type was calculated by averaging assigned values across reactors. These average values were then normalized to the sham control for the purposes of comparison.

Staining distribution/tissue level organization of each staining was similarly evaluated by assigning the distribution of observed medial layer a value on a scale of 0-3, with 0 representing even staining throughout the mural layer and increasing numbers representing increasing levels of spatial variation in staining distribution within the mural layer. Following quantification of each graft formulation within each of the four reactor experiments, the average tissue level organization of staining for a given graft type was calculated by averaging assigned values across reactors. These average values were then normalized to the sham control for the purposes of comparison.

2.5.2. Semi-quantitative assessment of elastic fiber disruption as a measure of neointima—The degree of neointima formation associated with the various graft formulations was assessed semi-quantitatively per standard methods.[31–34] Specifically, neointima formation is associated with disruption of the regular laminar structure of elastic fibers within the vessel wall. The degree of this disruption can be taken as a measure of the degree of intimal hyperplasia. Towards this end, the thickness of the disrupted elastic fiber layers was measured using the "measurement tool" of Adobe Photoshop software at three randomly selected locations within each fluorescently imaged arterial cryosection. Each thickness was divided by the corresponding thickness of the medial layer of vessel wall, excluding the adventitia. For arterial section, the average of the resulting three intima:media ratios was recorded as a measure of intimal hyperplasia for that section. Following quantification of each graft formulation within each of the four reactor experiments, the average degree of intimal hyperplasia for a given graft type was calculated by averaging assigned values across reactors. These average values were then normalized to the sham control for the purposes of comparison.

2.6 Oxidative degradation and mechanical testing

Accelerated oxidative degradation testing was utilized to assess the biostability of the electrospun outer layer. Composite vascular grafts of high, medium, and low compliance (n = 4 for each) were placed in an oxidative solution of 0.1M $CoCl_2$ and 20% H_2O_2 for 36 days at 37°C with solution changes every 3 days to maintain a relatively constant concentration of radicals. The effect of the oxidative treatment on the graft compliance, burst pressure, suture retention strength, fiber morphology, and surface chemistry was then characterized. Compliance was measured by first inserting latex tubes into 5 mm long graft segments and connecting to a syringe pump with a flow rate of 2 ml/min. The diameter of the graft was measured using a laser micrometer (1210 Laser Micrometer, Z-Mike) at 80 and 120 mmHg. Compliance (C) was calculated by $C = \Delta D/D_0 \bullet \Delta P = (D_{120} - D_{80})/D_{80} \bullet 40$ where D is the inner diameter [5]. Flow rate was then increased to 50 ml/min with obstructed flow until the outer layer burst. The highest pressure measured at the first sign of graft bursting was recorded as the burst pressure. Graft composites were cut lengthwise on one side and a suture was looped through the mesh 2 mm from one end in the center of the mesh. The un-sutured end was secured in the bottom clamp and the top suture was secured in the upper clamp. Uniaxial strain was applied at a rate of 100 mm/min using an Instron 3345 until the suture was pulled through the mesh. The maximum applied force was recorded as the suture retention strength.

The effect of oxidative degradation on the polyurethane mesh on surface chemistry and topography was determined using attenuated total reflectance- Fourier transform infrared (ATR-FTIR) spectroscopy and scanning electron microscopy (SEM). Meshes were washed and dried under vacuum overnight prior to testing (n = 4). Spectra were recorded using a Nicolet iS10 (Thermo Scientific) FTIR spectrometer at a resolution of 2 cm^{-1} for 64 scans using an ATR accessory with a germanium crystal. The fiber morphology was observed using SEM (Phenom Pro, NanoScience Instruments) at 10 kV accelerating voltage. Specimens approximately 5 mm × 5 mm were cut from each sample and mounted with conducting carbon tape on a cylindrical SEM stub (n = 4). Prior to imaging, the specimens

were coated with 4 nm of gold using a sputter coater (Sputter Coater 108, Cressington Scientific Instruments).

2.7. Statistical Analysis

Comparisons between two groups were performed using a two-tailed student's t-test. Comparisons between three or more groups were performed using ANOVA with a post-hoc Tukey's test. Significance was determined as $p<0.05$.

3. RESULTS

3.1. Varying graft compliance

We have previously demonstrated the ability to fabricate multilayer vascular grafts with improved compliance matching comparable to saphenous vein [7]. In this study, grafts were fabricated to approximate both low compliance synthetic grafts such ePTFE and the high compliance of native arteries independent of other factors such as graft chemistry and cellular interactions. To this end, Bionate® segmented polyurethane was electrospun with careful control of graft thickness and fiber morphology to meet target compliance values. Increasing electrospinning collection time from 2 hours to 6 hours resulted in grafts that were 0.4, 0.3, 0.2, and 0.1 mm thick with corollary compliances of 3.4 ± 1.1, 4.1 ± 0.3, 7.3 ± 1.3, and 8.1 ± 0.3 %/mmHg × 10^{-2}, respectively. These thicknesses yielded burst pressures of 2077 ± 284, 1542 ± 236, 1351 ± 244, and 1251 ± 260 mmHg, and suture retention strengths of 408 ± 16, 312 ± 24, 286 ± 40, and 193 ±13 gF, respectively. The measured compliance of the ePTFE control, determined by the same methodology, was 1.6 ± 0.2 %/mmHg × 10^{-2} and the carotid artery was measured to be 7.8 ± 0.2 %/mmHg × 10^{-2}, which was in good agreement with literature values [5, 35].

Given the strong correlation of mesh thickness and resulting graft compliance, we tuned thickness of candidate grafts to achieve target values. A low compliance graft to mimic the ePTFE clinical control (~2 ± 0.2 %/mmHg × 10^{-2}, 0.45 ± 0.02 mm thick), medium compliance graft to mimic the saphenous vein (~5.1 ± 0.8 %/mmHg × 10^{-2}, 0.26 ± 0.01 mm thick), and high compliance graft to mimic native carotid artery (~8.1 ± 0.3 %/mmHg × 10^{-2}, 0.1 ± 0.02 mm thick) were fabricated for use in the *ex vivo* bioreactor system (Figure 1 A, B). The fiber diameter was kept constant with average fiber diameters for the low, medium, and high compliance grafts of 2.04 ± 0.29, 1.97 ± 0.29, and 1.94 ± 0.33 μm, respectively. The grafts retained appropriate burst pressures and suture retention strengths, comparable to the saphenous vein graft used clinically (Figure 1 C, D). Electrospun meshes with target biomechanical properties were then coated with a poly(ethylene glycol)-based hydrogel to ensure thromboresistance in subsequent bioreactor studies [7]. This coating has been demonstrated to have a negligible effect on the compliance of the grafts, as shown in Supplementary Figure 1.

3.2 Computational modeling

A computational model was created to illustrate the changes in flow as a function of compliance and estimate the resulting changes in wall shear stress at the distal anastomosis of the high, medium, and low compliance grafts (Figure 2). Zones of recirculation were

apparent in the low compliance graft model with flow recirculation distal to the graft with a corollary wall shear stress of 0.03 N/m^2 at 80mmHg and 0.03 N/m^2 at 120 mmHg. These values approached zero near the zone of recirculation at the distal anastomosis. The observed zones of recirculation were reduced in the medium compliance model, with the wall shear stress calculated to be 1.04 N/m^2 at 80 mmHg and 1.08 N/m^2 at 120 mmHg. The high compliance graft eliminated zones of recirculation with wall shear stress calculated to be 3.46 N/m^2 at 80 mmHg and 3.60 N/m^2 at 120 mmHg.

3.4 Ex vivo bioreactor immunohistochemistry

The *ex vivo* bioreactor model allows for simplification of a complex *in vivo* system. In these bioreactor studies, previously validated culture formats which allowed for sustained vessel viability as well as for assessment of structural changes were used as a design basis [42–45]. In general, the arteries sutured to the low compliance grafts and the ePTFE controls exhibited similar staining for early markers of intimal hyperplasia, whereas the arteries sutured to the high compliance grafts displayed similar staining as the artery-artery sham controls.

In comparing VSMC phenotype, greater spatial heterogeneity in the staining for contractile protein SMa-actin within the medial layer was observed in the lower compliance groups relative to the sham control (Figure 4). In addition, regions of intense staining for the contractile protein SM22α (Figure 4) as well as for the proliferation marker Ki67 and the cell-cell adhesion molecule N-Cadherin (Figure 5) within the medial layer were noted with increasing intensity and frequency with decreasing graft compliance.

In contrast, staining for N-Cadherin in the endothelium – where it regulates endothelial cell-VMSC interactions - was increased in all synthetic graft groups relative to the sham control (Figure 6), although the increase was modest for the high compliance group. Similarly, no differences in staining for endothelial cell junction protein VE-Cadherin were observed across groups. However, staining for the proinflammatory/prothrombotic marker vWF displayed a clear and consistent increase with higher degrees of compliance mismatch. Furthermore, the low compliance treatment group and ePTFE control group demonstrated vWF staining penetrating into the vessel wall, as is often observed in intimal hyperplasia due to the release of soluble vWF by the endothelium [46–48].

To examine alterations in medial layer extracellular matrix associated with these differences in VMSC and endothelial cell behavior, staining for “acute” intimal hyperplasia markers MMP-1 and versican was conducted (Figure 7). MMP-1 staining – particularly in the intimal space – increased as graft compliance decreased. Similarly, versican staining displayed higher overall intensity as well as increased spatial variation in the lower compliance treatment groups. Semi-quantitative assessments of mural staining – both of staining intensity and staining distribution - for SMα-actin, SM22α, Ki67, N-Cadherin, MMP-1 and versican support the above qualitative observations (Supplementary Figure 5 A,B). Increased intimal thickening with decreasing graft compliance was also observed through assessment of elastic fibers via autofluorescence (Figure 7). In particular, semi-quantitative assessment of the average intima:media ratio across treatment groups supported increased levels of intimal hyperplasia with increased levels of graft-host compliance mismatch (Figure 8).

3.3 Biostability of Synthetic Grafts

As a final evaluation, accelerated degradation testing was performed to confirm the biostability of the vascular grafts and retention of biomechanical properties. Accelerated oxidative degradation in 0.1M $CoCl_2$ and 20% H_2O_2 for 36 days at 37°C was selected for its well-established use in mimicking macrophage-mediated oxidative degradation of polyurethanes. The compliance for the high, medium, and low compliance grafts were not significantly different after degradative treatment, Figure 9A. Similarly, the burst pressures were not significantly different for the high and medium compliance grafts; however, a small but significant loss of burst pressure was observed for the low compliance graft (Figure 9B). The suture retention strength for the grafts also remained largely unaltered by degradative treatment (Figure 9C). No notable change in fiber morphology of the meshes was observed with scanning electron microscopy and no notable change in surface chemistry as monitored with ATR-FTIR spectroscopy was observed after degradative treatment. There was some salt precipitate apparent in the treated samples even after washing and drying (Figure 9D,E). Overall, the biomechanical properties of the vascular grafts were retained after accelerated oxidative degradation.

4. DISCUSSION

Loss of patency due to intimal hyperplasia remains a leading cause of failure of small diameter synthetic grafts [5]. It has long been hypothesized that intimal hyperplasia develops at the distal anastomosis due to compliance mismatch between the low compliance synthetic graft and the high compliance artery [5]. However, it has been difficult to isolate compliance as the single factor affecting arterial remodeling that defines intimal hyperplasia. In this study, we were able to uniquely modulate compliance independent of graft surface topology or graft chemistry. The grafts also retained sufficient burst pressure and suture retention strength for implantation, comparable to that of the saphenous vein (Figure 1). As such, these grafts allow for the isolation of compliance as the single effector of change. Low, medium, and high compliance grafts were fabricated such that the low compliance graft was comparable to the ePTFE clinical control and the high compliance graft was comparable to the native carotid artery (Figure 1B). This range of distinct compliances allowed for targeted analysis of changes induced by compliance mismatch and relevant to grafts in current clinical use.

After developing grafts of these target compliances, a computational model was used to analyze blood flow disruptions due to compliance mismatch. Although this is a simple and idealized model, it provides a means to isolate and estimate the effect of the compliance-graft mismatch on changes in blood flow, which are hypothesized to initiate intimal thickening. The computational model demonstrated changes in the blood flow profile and corollary changes in wall shear stress between grafts of different compliances (Figure 2). Here, we are able to demonstrate that the low compliance grafts have the greatest difference in diameter and the largest corresponding effect on the blood flow profile, creating zones of blood recirculation and low wall shear stresses. As compliance increases to that of the high compliance graft, the dilation changes between the graft and the native artery decrease, preserving flow lines and increasing wall shear stress. Previous studies performed by Sho et

al. in a rabbit model provides context for these predicted wall shear stresses and correlation with intimal thickening. In this study, an arteriovenous shunt was used to isolate the effect of blood flow rate on intimal thickening and demonstrated an increase in intimal thickening when wall shear stress fell below approximately 0.5 N/m^2 [50]. We utilized this value as a rough threshold value for which of the grafts would likely initiate intimal thickening. The wall shear stress that was associated with the low compliance graft (0.03 N/m^2) fell well below the described threshold for intimal thickening; whereas, the medium compliance graft displayed a similar wall shear stress (1.04 N/m^2) and the high compliance graft resulted in a much higher wall shear stress (3.6 N/m^2). Based on this correlation, it is expected that grafts with low compliance, such as Dacron® or Goretex®, will induce intimal hyperplasia based on the computational model predictions and grafts with higher compliance may mitigate those effects. In addition, the medium compliance graft provides an approximation of the wall shear stress of saphenous vein grafts due to similar compliance values (~4.5 %/mmHg $\times 10^{-2}$) [39]. The reduced wall shear stress of the medium compliance graft to approximately the threshold value for intimal thickening corresponds well with the reduction in patency in clinical bypass procedures as compared to mammary artery grafts that are more similar to the high compliance grafts of this study [38, 51].

In agreement with this prediction, the arteries sutured to grafts of low and medium compliance demonstrated changes in early markers of intimal hyperplasia after two weeks of culture under physiological conditions (Figures 4–7). For instance, regional increases in VSMC expression of Ki67 and N-Cadherin are associated with intimal thickening, and inhibition of N-Cadherin function has been shown to suppress VSMC migration and intimal growth. Similarly, increases in endothelial cell N-Cadherin and vWF expression and presence of diffused vWF within the arterial wall have been consistently linked to early intimal hyperplasia [46–48]. In terms of extracellular matrix, the regional alterations in MMP-1 and versican levels observed in the present culture model are also repeatedly observed in acute intimal hyperplasia [15, 52]. In particular, increased deposition of proteoglycans such as versican and biglycan are linked to the VSMC phenotypic switch from contractile to proliferative in early intimal hyperplasia [14, 15, 17, 19, 20, 53]. Furthermore, broad spectrum inhibition of MMP activity has previously been shown to reduce intimal hyperplasia in a porcine model [54]. Beyond changes in versican, imaging of elastic fibers allowed for clear visualization of increased intimal thickening with increase vessel-graft compliance mismatch.

Together, the changes in markers of intimal hyperplasia in the low and medium compliance grafts correlate well to the prediction of lower wall shear stress in these grafts compared to the high compliance graft. All of these findings indicate causation between graft compliance and intimal hyperplasia. The findings also identify a graft with compliance matching that may limit intimal hyperplasia, one of the first grafts demonstrated to do so.

The computational model and ex vivo bioreactor system would both benefit from correlation to *in vivo* evaluation of compliance mismatch in order to demonstrate that the trends demonstrated in the short term model are maintained in the long term. Therefore, the grafts must demonstrate the biostability required for implantation safety for a large animal model. The accelerated oxidative degradation demonstrated no major changes in graft fiber

morphology, surface chemistry, or mechanical properties, including compliance (Figure 9). These findings in combination with previous studies that confirmed the thromboresistance of the multilayer grafts support the safety of the constructs for long-term implantation studies [7]. Notable for the continuation of this work is that these findings indicate that the compliance would remain constant over the extended *in vivo* evaluation needed to assess intimal hyperplasia.

Although the studies presented here provide valuable insights into a previously speculated problem, there are study limitations worth noting. In particular, the computational model is a relatively simplified view of the complex fluid-material interactions in both the *ex vivo* bioreactor and clinical use. The simulation is limited by the use of solid walls and no fluid-structure interactions in the model. Future iterations of this model should account for surface roughness differences, pulsatile flow, and geometric irregularities due to anastomosis. The effect of flow rate is also an additional area of study to better correlate between bioreactor, computational models, and clinical use. In the current study, the bioreactor study was performed at the relatively low flow rates typical of ex vivo carotid artery bioreactors;[29, 30] whereas, the computational model used flow rates relevant to the coronary artery [28]. A comparison of the modeled fluid dynamics at the distal anastomosis of the low compliance graft at these two flow rates indicated similar zones of recirculation and low wall shear stress (Supplementary Figure 6). This suggests that the findings of this study are relevant at a range of physiological flow rates. Finally, the study is also somewhat limited by the timepoints of the bioreactor study due to the challenges in maintaining an ex vivo organ culture model. Intermediate time points in the two-week study may provide additional insight into the progression of intimal hyperplasia. Despite these limitations, this initial evaluation and simple model yields a rough demonstration of flow changes as a function of graft compliance.

5. CONCLUSION

Intimal hyperplasia contributes to the high failure rates of synthetic vascular grafts currently available to clinicians. Elucidating the mechanism that graft compliance mismatch initiates intimal hyperplasia has been clinically difficult due to many confounding factors such as varying graft compositions and confounding diseases. Despite some of these challenges, low wall shear stress has been indicated as a cause of intimal thickening. It has been historically theorized that the compliance mismatch between the vascular graft and the native vasculature disrupts blood flow and creates zones of blood recirculation. Our ability to fabricate grafts with varying compliance independent of other variables allowed for a direct correlation of changes in wall shear stress due to poor compliance matching and early markers of intimal hyperplasia in a novel *ex vivo* organ culture model. The tools we have developed for these studies not only enable the investigation of intimal hyperplasia, they also allow for efficient future graft design iterations. The computational model also allows for optimization of graft parameters to limit turbulent flow and maintain high wall shear stress at the distal anastomosis. Future versions of the computational model could include more complex arterial geometries and anastamoses to better predict flow and wall shear stress *in vivo.* Finally, the *ex vivo* system can be used to quickly screen vascular graft prototypes for their propensity to induce early markers of intimal hyperplasia. Future work will build on

the current studies by examining the long term effects of compliance mismatch in a large animal model and correlate these findings to the *ex vivo* bioreactor screening.

Supplementary Material

Refer to Web version on PubMed Central for supplementary material.

ACKNOWLEDGEMENTS

The work presented here was supported by the Texas A&M University Diversity Fellowship and the National Institutes of Health R21 EB020978 and R01 EB013297. The Bionate® segmented polyurethane was provided by DSM Biomedical (Exton, PA).

REFERENCES

[1]. Benjamin EJ, Blaha MJ, Chiuve SE, Cushman M, Das SR, Deo R, de Ferranti SD, Floyd J, Fomage M. Heart disease and stroke statistics—2017 update: a report from the American Heart Association. Circulation 2017;135:el46.

[2]. Greenwald S, Berry C. Improving vascular grafts: the importance of mechanical and haemodynamic properties. The Journal of pathology 2000;190:292–9. [PubMed: 10685063]

[3]. Lemson M, Tordoir J, Daemen M, Kitslaar P. Intimal hyperplasia in vascular grafts. European Journal of Vascular and Endovascular Surgery 2000;19:336–50. [PubMed: 10801366]

[4]. Wang X, Lin P, Yao Q, Chen C. Development of Small-Diameter Vascular Grafts. World Journal of Surgery 2007;31:682–9. [PubMed: 17345123]

[5]. Salacinski HJ, Goldner S, Giudiceandrea A, Hamilton G, Seifalian AM, Edwards A, Carson RJ. The mechanical behavior of vascular grafts: a review. Journal of biomaterials applications 2001;15:241–78. [PubMed: 11261602]

[6]. Haruguchi H, Teraoka S. Intimal hyperplasia and hemodynamic factors in arterial bypass and arteriovenous grafts: a review. Journal of Artificial Organs 2003;6:227–35. [PubMed: 14691664]

[7]. Browning M, Dempsey D, Guiza V, Becerra S, Rivera J, Russell B, Hook M, Clubb F, Miller M, Fossum T. Multilayer vascular grafts based on collagen-mimetic proteins. Acta biomaterialia 2012;8:1010–21. [PubMed: 22142564]

[8]. Nezarati RM, Eifert MB, Dempsey DK, Cosgriff-Hernandez E. Electrospun vascular grafts with improved compliance matching to native vessels. Journal of Biomedical Materials Research PartB: Applied Biomaterials 2015;103:313–23. [PubMed: 24846218]

[9]. Antoniadis AP, Mortier P, Kassab G, Dubini G, Foin N, Murasato Y, Giannopoulos AA, Tu S, Iwasaki K, Hikichi Y. Biomechanical modeling to improve coronary artery bifurcation stenting: expert review document on techniques and clinical implementation. JACC: Cardiovascular Interventions 2015;8:1281–96. [PubMed: 26315731]

[10]. Karanasiou GS, Papafaklis MI, Conway C, Michalis LK, Tzafriri R, Edelman ER, Fotiadis DI. Stents: biomechanics, biomaterials, and insights from computational modeling. Annals of biomedical engineering 2017;45:853–72. [PubMed: 28160103]

[11]. Lally C, Dolan F, Prendergast P. Cardiovascular stent design and vessel stresses: a finite element analysis. Journal of biomechanics 2005;38:1574–81. [PubMed: 15958213]

[12]. Rashid ST, Salacinski HJ, Hamilton G, Seifalian AM. The use of animal models in developing the discipline of cardiovascular tissue engineering: a review. Biomaterials 2004;25:1627–37. [PubMed: 14697864]

[13]. Rzucidlo EM, Martin KA, Powell RJ. Regulation of vascular smooth muscle cell differentiation. J Vase Surg 2007;45 Suppl A:A25–32.

[14]. Chen PY, Qin L, Li G, Tellides G, Simons M. Fibroblast growth factor (FGF) signaling regulates transforming growth factor beta (TGFbeta)-dependent smooth muscle cell phenotype modulation. Scientific reports 2016;6:33407. [PubMed: 27634335]

[15]. Newby AC, Zaltsman AB. Molecular mechanisms in intimal hyperplasia. J Pathol 2000;190:300–9. [PubMed: 10685064]

[16]. Ataya B, Tzeng E, Zuckerbraun BS. Nitrite-generated nitric oxide to protect against intimal hyperplasia formation. Trends in cardiovascular medicine 2011;21:157–62. [PubMed: 22814422]

[17]. Davies MG, Hagen PO. Pathobiology of intimal hyperplasia. The British journal of surgery 1994;81:1254–69. [PubMed: 7953384]

[18]. Lyon CA, Koutsouki E, Aguilera CM, Blaschuk OW, George SJ. Inhibition of N-cadherin retards smooth muscle cell migration and intimal thickening via induction of apoptosis. Journal of vascular surgery 2010;52:1301–9. [PubMed: 20630685]

[19]. Jennette JC, Stone JR. Chapter 11 - Diseases of Medium-Sized and Small Vessels Cellular and Molecular Pathobiology of Cardiovascular Disease. San Diego: Academic Press; 2014 p. 197–219.

[20]. Mills B, Robb T, Larson DF. Intimal hyperplasia: slow but deadly. Perfusion 2012;27:520–8. [PubMed: 22751382]

[21]. Ferreri DM, Minnear FL, Yin T, Kowalczyk AP, Vincent PA. N-cadherin levels in endothelial cells are regulated by monolayer maturity and p120 availability. Cell communication & adhesion 2008;15:333–49. [PubMed: 18979298]

[22]. Sabatini PJ, Zhang M, Silverman-Gavrila R, Bendeck MP, Langille BL. Homotypic and endothelial cell adhesions via N-cadherin determine polarity and regulate migration of vascular smooth muscle cells. Circulation research 2008;103:405–12. [PubMed: 18617695]

[23]. Wang Y, Liang A, Luo J, Liang M, Han G, Mitch WE, Cheng J. Blocking Notch in endothelial cells prevents arteriovenous fistula failure despite CKD. Journal of the American Society of Nephrology 2014;25:773–83. [PubMed: 24480830]

[24]. Miyachi H, Takahashi M, Komori K. A Novel Approach against Vascular Intimal Hyperplasia Through the Suppression of Girdin. Annals of vascular diseases 2015;8:69–73. [PubMed: 26131024]

[25]. Hahn MS, Taite LJ, Moon JJ, Rowland MC, Ruffino KA, West JL. Photolithographic patterning of polyethylene glycol hydrogels. Biomaterials 2006;27:2519–24. [PubMed: 16375965]

[26]. Cho YI, Kensey KR. Effects of the non-Newtonian viscosity of blood on flows in a diseased arterial vessel. Part 1: Steady flows. Biorheology 1991;28:241–62. [PubMed: 1932716]

[27]. Johnston BM, Johnston PR, Corney S, Kilpatrick D. Non-Newtonian blood flow in human right coronary arteries: steady state simulations. Journal of biomechanics 2004;37:709–20. [PubMed: 15047000]

[28]. Ackroyd N, Gill R, Griffiths K, Kossoff G, Appleberg M. Quantitative common carotid artery blood flow: prediction of internal carotid artery stenosis. Journal of vascular surgery 1986;3:846–53. [PubMed: 2940377]

[29]. Lu X, Kassab GS. Nitric oxide is significantly reduced in ex vivo porcine arteries during reverse flow because of increased superoxide production. The Journal of physiology 2004;561:575–82. [PubMed: 15579542]

[30]. Mundargi R, Venkataraman D, Kumar S, Mogal V, Ortiz R, Loo J, Venkatraman S, Steele T. Novel Sensor-Enabled Ex Vivo Bioreactor: A New Approach towards Physiological Parameters and Porcine Artery Viability. BioMed research international 2015;2015:958170. [PubMed: 26609536]

[31]. Holt CM, Francis SE, Newby AC, Rogers S, Gadsdon PA, Taylor T, Angelini GD. Comparison of response to injury in organ culture of human saphenous vein and internal mammary artery. The Annals of thoracic surgery 1993;55:1522–8. [PubMed: 8512406]

[32]. Huang L, Zhang SM, Zhang P, Zhang XJ, Zhu LH, Chen K, Gao L, Zhang Y, Kong J, Tian S. Interferon regulatory factor 7 protects against vascular smooth muscle cell proliferation and neointima formation. Journal of the American Heart Association 2014;3:e001309. [PubMed: 25304854]

[33]. Lipskaia L, Hadri L, Le Prince P, Esposito B, Atassi F, Liang L, Glorian M, Limon I, Lompre A, Lehoux S. SERCA2a gene transfer prevents intimal proliferation in an organ culture of human internal mammary artery. Gene therapy 2013;20:396. [PubMed: 22763406]

[34]. Perrée J, van Leeuwen TG, Kerindongo R, Spaan JA, VanBavel E. Function and structure of pressurized and perfused porcine carotid arteries: effects of in vitro balloon angioplasty. The American journal of pathology 2003;163:1743–50. [PubMed: 14578174]

[35]. Abbott WM, Megerman J, Hasson JE, L'ltalien G, Warnock DF. Effect of compliance mismatch on vascular graft patency. Journal of vascular surgery 1987;5:376–82. [PubMed: 3102762]

[36]. Mine Y, Mitsui H, Oshima Y, Noishiki Y, Nakai M, Sano S. Suture retention strength of expanded polytetrafluoroethylene (ePTFE) graft. Diss Okayama University 2010.

[37]. Zhang L, Ao Q, Wang A, Lu G, Kong L, Gong Y, Zhao N, Zhang X. A sandwich tubular scaffold derived from chitosan for blood vessel tissue engineering. Journal of biomedical materials research Part A 2006;77:277–84. [PubMed: 16400655]

[38]. Konig G, McAllister TN, Dusserre N, Garrido SA, Iyican C, Marini A, Fiorillo A, Avila H, Wystrychowski W, Zagalski K, Maruszewski M, Jones A, Cierpka AL, Lech de la Fuente L, L'Heureux N. Mechanical properties of completely autologous human tissue engineered blood vessels compared to human saphenous vein and mammary artery. Biomaterials 2009;30:1542–50. [PubMed: 19111338]

[39]. Walden R, Gilbert J, Megerman J, Abbott WM. Matched elastic properties and successful arterial grafting. Archives of Surgery 1980;115:1166–9. [PubMed: 6448593]

[40]. Wang C, Cen L, Yin S, Liu Q, Liu W, Cao Y, Cui L. A small diameter elastic blood vessel wall prepared under pulsatile conditions from polyglycolic acid mesh and smooth muscle cells differentiated from adipose-derived stem cells. Biomaterials 2010;31:621–30. [PubMed: 19819545]

[41]. Mun CH, Jung Y, Kim SH, Kim HC, Kim SH. Effects of Pulsatile Bioreactor Culture on Vascular Smooth Muscle Cells Seeded on Electrospun Poly (lactide- co- ε- caprolactone) Scaffold. Artificial organs 2013;37:E168–E78. [PubMed: 23834728]

[42]. Berard X, Déglise S, Alonso F, Saucy F, Meda P, Bordenave L, Corpataux JM, Haefliger JA. Role of hemodynamic forces in the ex vivo arterialization of human saphenous veins. Journal of vascular surgery 2013;57:1371–82. [PubMed: 23351647]

[43]. Li L, Terry CM, Blumenthal DK, Kuji T, Masaki T, Kwan BC, Zhuplatov I, Leypoldt JK, Cheung AK. Cellular and morphological changes during neointimal hyperplasia development in a porcine arteriovenous graft model. Nephrology Dialysis Transplantation 2007;22:3139–46.

[44]. Riches K, Angelini TG, Mudhar GS, Kaye J, Clark E, Bailey MA, Sohrabi S, Korossis S, Walker PG, Scott DJA. Exploring smooth muscle phenotype and function in a bioreactor model of abdominal aortic aneurysm. Journal of translational medicine 2013; 11:208. [PubMed: 24028184]

[45]. Yazdani SK, Berry JL. Development of an in vitro system to assess stent-induced smooth muscle cell proliferation: a feasibility study. Journal of Vascular and Interventional Radiology 2009;20:101–6. [PubMed: 19028120]

[46]. De Meyer GR, Hoylaerts MF, Kockx MM, Yamamoto H, Herman AG, Bult H. Intimal deposition of functional von Willebrand factor in atherogenesis. Arteriosclerosis, thrombosis, and vascular biology 1999;19:2524–34.

[47]. Qin F, Dardik H, Pangilinan A, Robinson J, Chuy J, Wengerter K. Remodeling and suppression of intimal hyperplasia of vascular grafts with a distal arteriovenous fistula in a rat model. Journal of vascular surgery 2001;34:701–6. [PubMed: 11668327]

[48]. Rand JH, Badimon L, Gordon RE, Uson RR, Fuster V. Distribution of von Willebrand factor in porcine intima varies with blood vessel type and location. Arteriosclerosis, Thrombosis, and Vascular Biology 1987;7:287–91.

[49]. Dempsey DK, Carranza C, Chawla CP, Gray P, Eoh JH, Cereceres S, Cosgriff-Hernandez EM. Comparative analysis of in vitro oxidative degradation of poly (carbonate urethanes) for biostability screening. Journal of Biomedical Materials Research Part A 2014;102:3649–65. [PubMed: 24265203]

[50]. Sho E, Nanjo H, Sho M, Kobayashi M, Komatsu M, Kawamura K, Xu C, Zarins CK, Masuda H. Arterial enlargement, tortuosity, and intimal thickening in response to sequential exposure to high and low wall shear stress. Journal of vascular surgery 2004;39:601–12. [PubMed: 14981455]

[51]. Goldman S, Zadina K, Moritz T, Ovitt T, Sethi G, Copeland JG, Thottapurathu L, Krasnicka B, Ellis N, Anderson RJ. Long-term patency of saphenous vein and left internal mammary artery grafts after coronary artery bypass surgery: results from a Department of Veterans Affairs Cooperative Study. Journal of the American College of Cardiology 2004;44:2149–56. [PubMed: 15582312]

[52]. Kenagy RD, Plaas AH, Wight TN. Versican degradation and vascular disease. Trends in cardiovascular medicine 2006;16:209–15. [PubMed: 16839865]

[53]. Talusan P, Bedri S, Yang S, Kattapuram T, Silva N, Roughley PJ, Stone JR. Analysis of intimal proteoglycans in atherosclerosis-prone and atherosclerosis-resistant human arteries by mass spectrometry. Molecular & Cellular Proteomics 2005;4:1350–7. [PubMed: 15970583]

[54]. Rotmans JI, Velema E, Verhagen HJ, Blankensteijn JD, de Kleijn DP, Stroes ES, Pasterkamp G. Matrix metalloproteinase inhibition reduces intimal hyperplasia in a porcine arteriovenous-graft model. Journal of vascular surgery 2004;39:432–9. [PubMed: 14743149]

Statement of Significance

We present an ex vivo organ culture model as a means to screen vascular grafts for early markers of intimal hyperplasia, a leading cause of small diameter vascular graft failure. Furthermore, a computational model was used to predict the effect of graft compliance on wall shear stress and then correlate these values to changes in arterial remodeling in the organ culture model. Combined, the ex vivo bioreactor system and computational model provide insight into the mechanistic relationship between graft-arterial compliance mismatch and the onset of intimal hyperplasia.

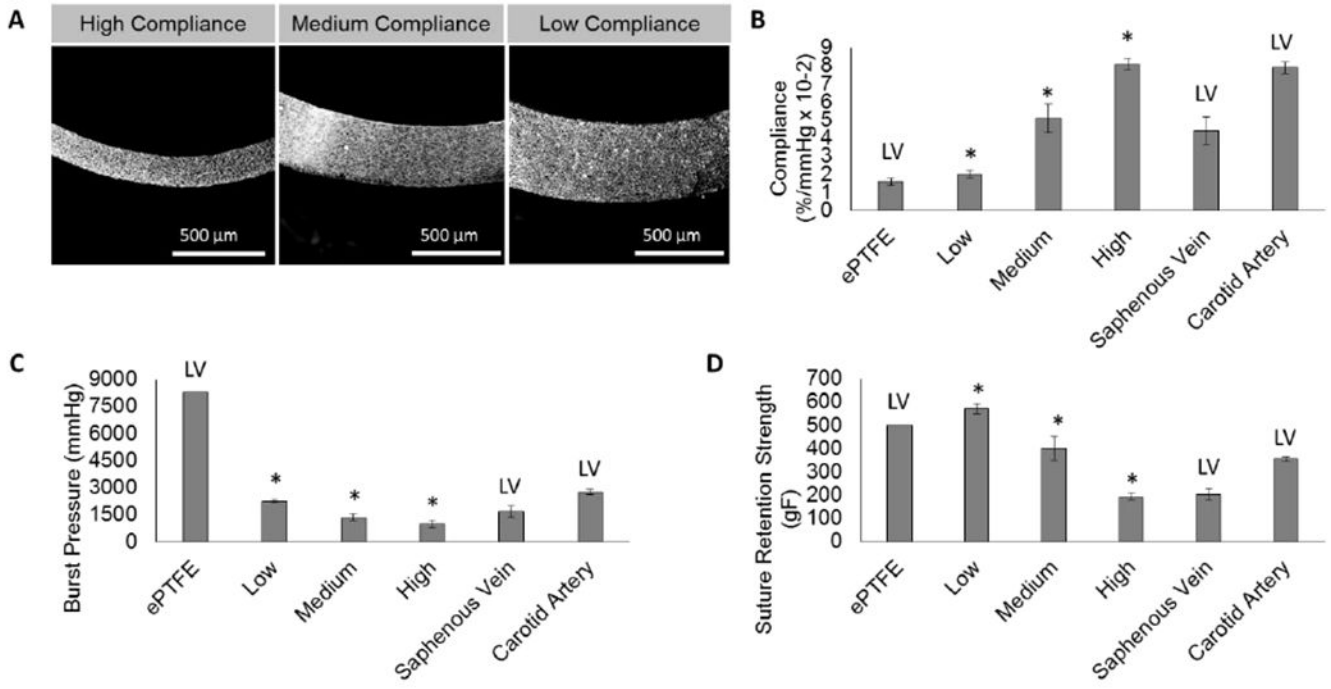

Figure 1:

A) Effect of modulating collection time on graft thickness as demonstrated by SEM. Compliance (B) and burst pressure (C), and suture retention strength (D) of the low, medium, and high compliance grafts compared to the clinical control ePTFE. Data is represented as average ± standard deviation for n=6. Statistical significance is shown by * showing significance from all other measured values, with $p<0.05$. LV: Literature values for ePTFE are from Salacinski et al., Mun et al., and Mine et al.; Saphenous Vein from Walden et al., Konig et al., and Wang et al.; and Carotid Artery from Abbot et al. and Zhang et al. [5, 35–41].

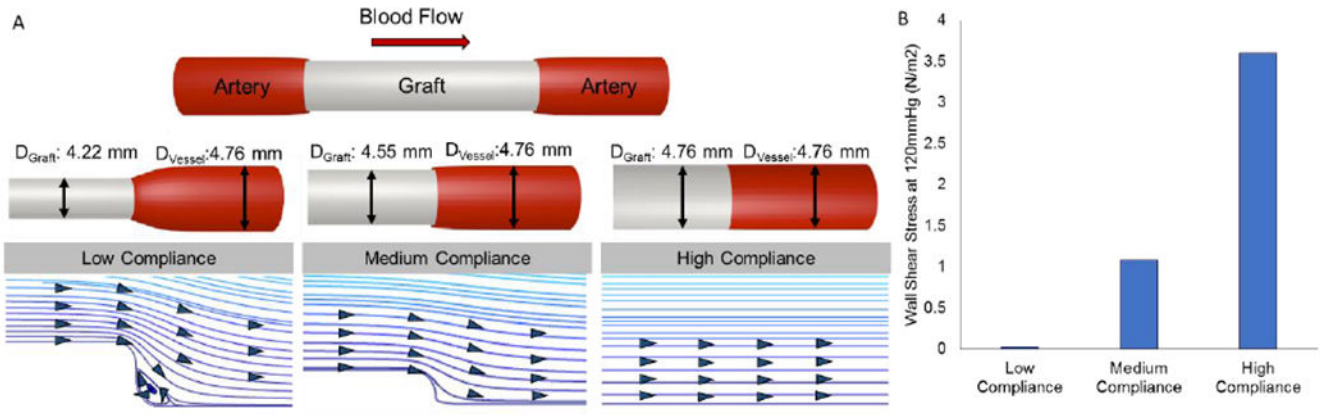

Figure 2:

A. Effect of compliance on flow patterns and wall shear stress at the distal anastomosis as determined by the idealized computational model made in COMSOL. Linear flow patterns demonstrate decreasing flow disruption with increasing compliance. B. Correlation of graft compliance and predicted wall shear stress at the distal anastomoses at 120 mmHg.

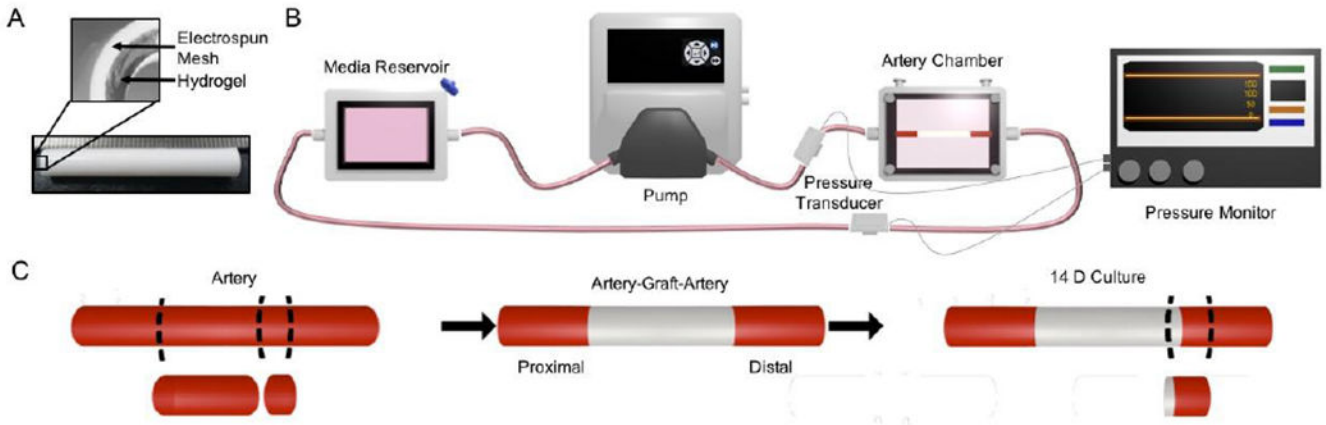

Figure 3:

A) Inner and outer layers of the multilayer graft. B) Ex vivo organ culture system. C) Arterial segment harvesting and artery-graft construction. The central segment was excised from each vessel and the distal 2-3 mm was preserved for “day 0” histology. Graft or arterial segment (sham) was inserted into the central region of each artery and flow initiated. Following 14 days of culture, flow was terminated and a 2-3 mm arterial segment at the distal anastomosis was harvested for histology. Cryosections that were between 1.2-1.7 mm from their respective distal graft-host anastomosis were utilized for immunostaining.

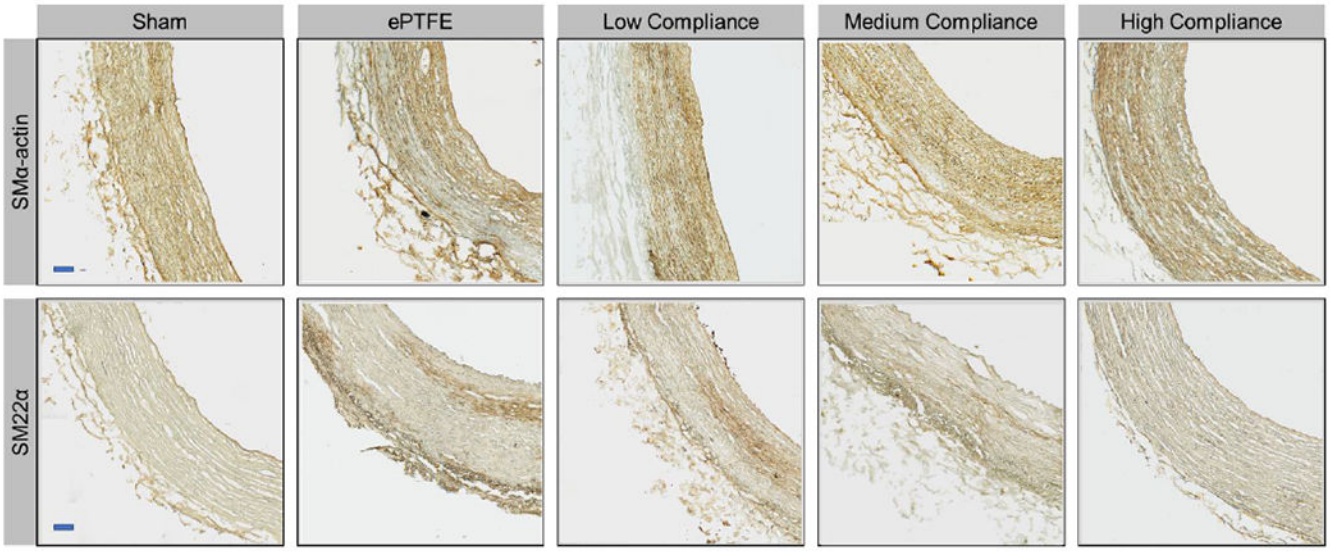

Figure 4:

The effect of compliance on smooth muscle cells at the distal anastamosis as demonstrated by histological staining of SMα-actin and SM22α at day 14. The images presented are representative of 4 independent bioreactor runs with at least two independent repeat immunostainings per treatment group. Blue scale bars = 100 mm and apply to all images in the respective series.

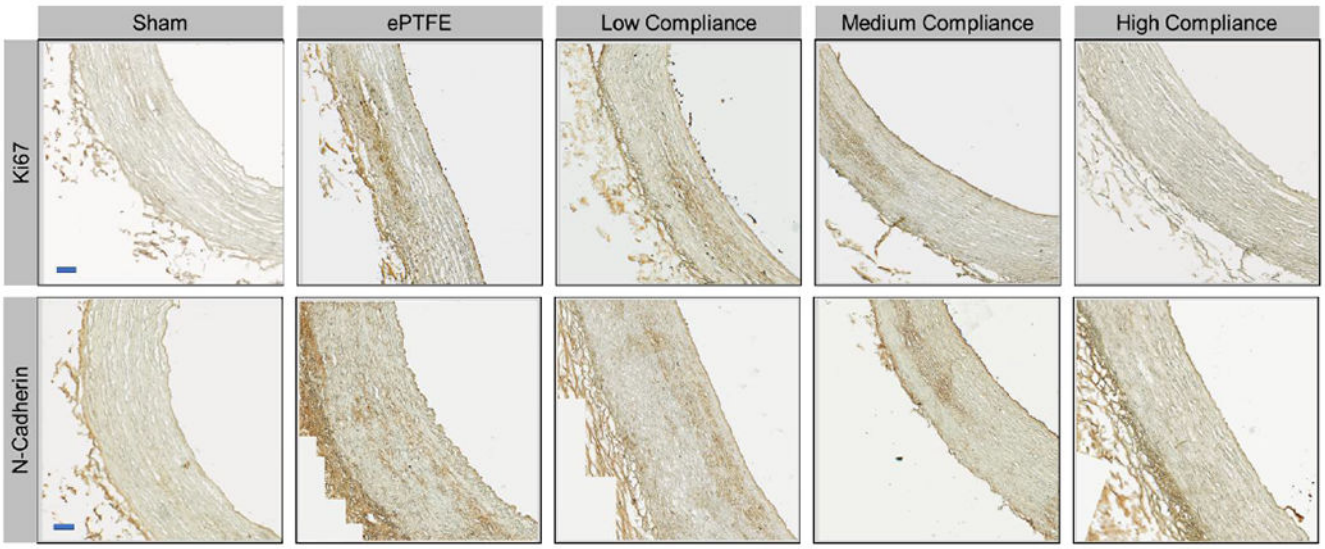

Figure 5:

The effect of compliance on the smooth muscle cells at the distal anastomosis by histological staining of Ki67 and N-Cadherin at day 14. The images presented are representative of 4 independent bioreactor runs with at least two independent repeat immunostainings per treatment group. Blue scale bars = 100 mm and apply to all images in the respective series.

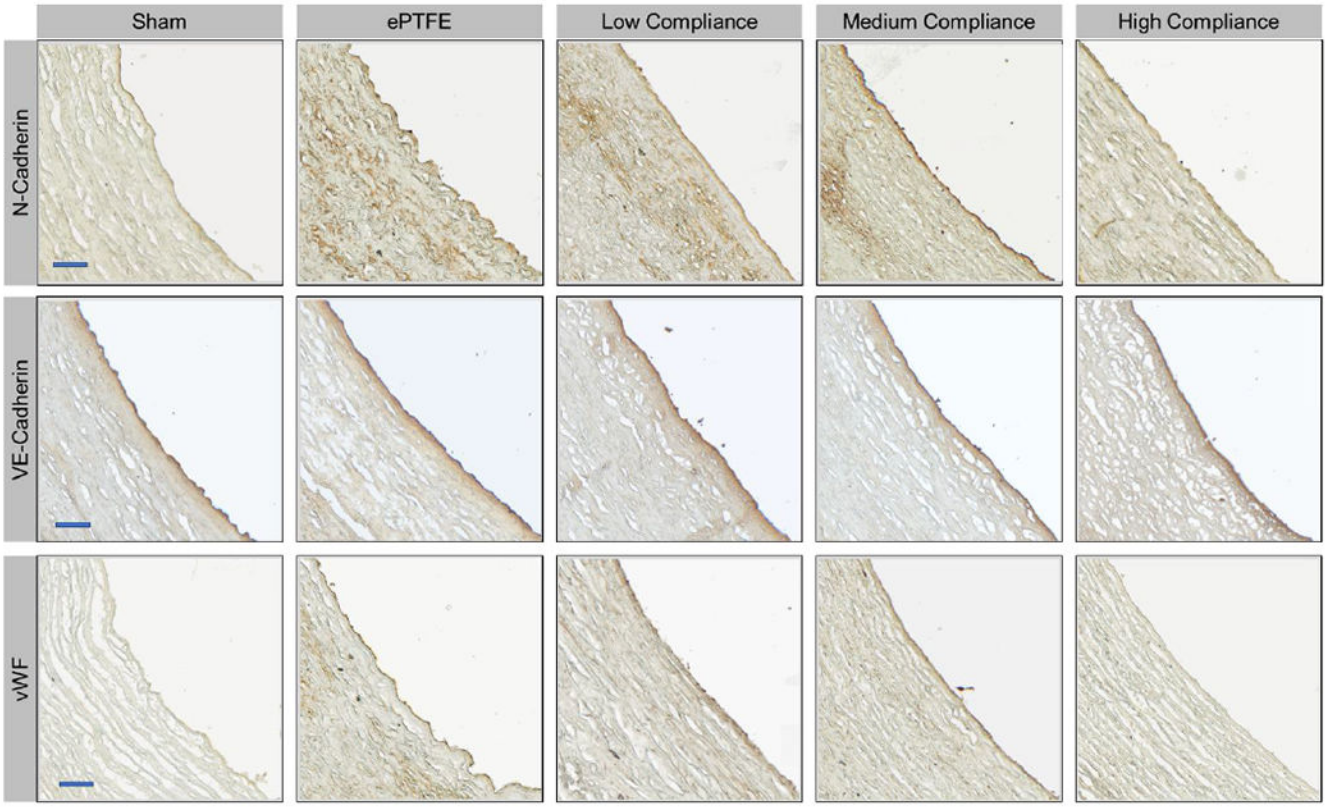

Figure 6:

The effect of compliance on endothelial cell behavior at the distal anastomosis by histological staining of N-cadherin, VE-Cadherin and vWF at day 14. Higher magnification images are provided to enhance the visibility of epithelial staining. The images presented are representative of 4 independent bioreactor runs with at least two independent repeat immunostainings per treatment group. Blue scale bars = 100 mm and apply to all images in the respective series.

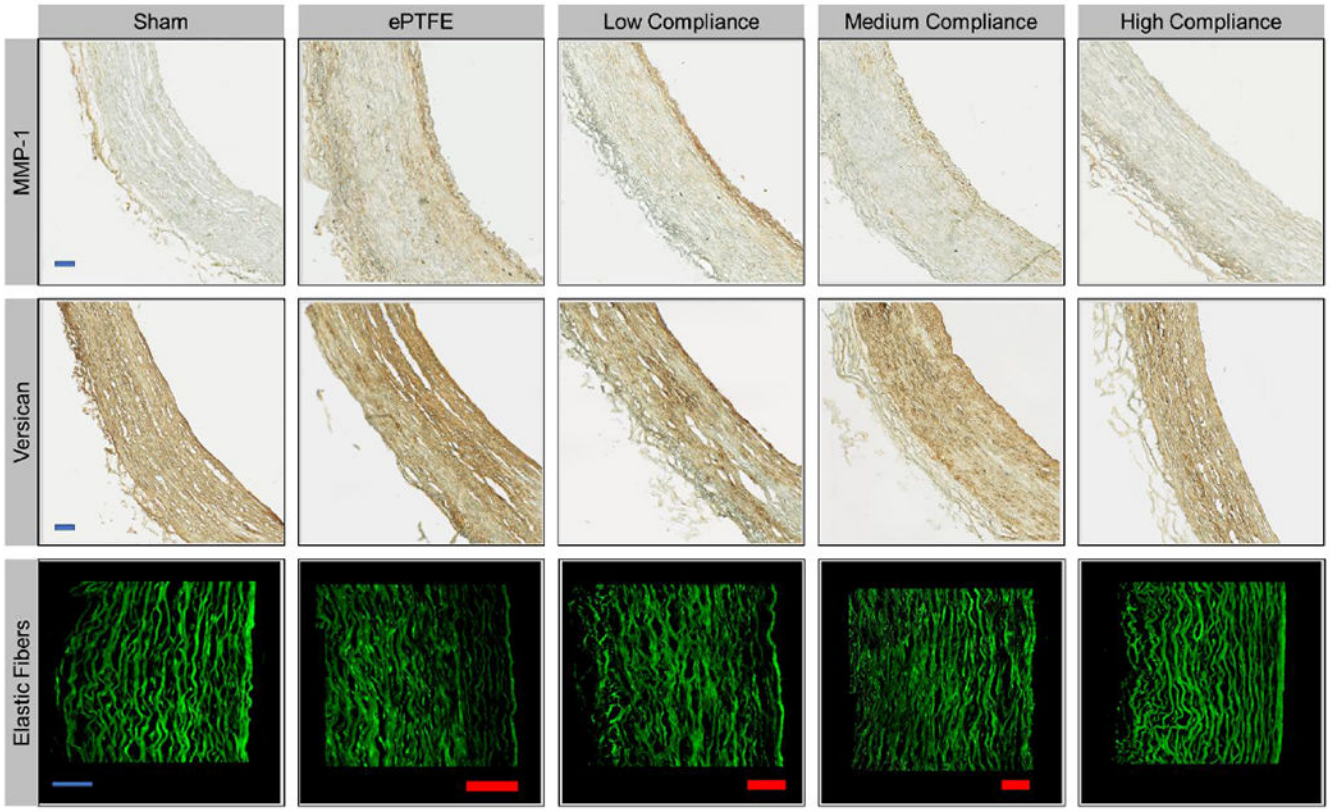

Figure 7:

The effect of compliance on the extracellular matrix of the vessel media at the distal anastomosis by histological staining of MMP-1 and versican at day 14 and autofluorescence of elastic fibers at day 14. The red bars underneath the medium compliance, low compliance, and ePTFE specimens indicate the extent of intimal thickening. Intimal thickening was not observed for the high compliance specimens or for the artery-artery sham controls. The images presented are representative of 4 independent bioreactor runs with at least two independent repeat immunostainings per treatment group. Blue scale bars =100 mm and apply to all images in the respective series.

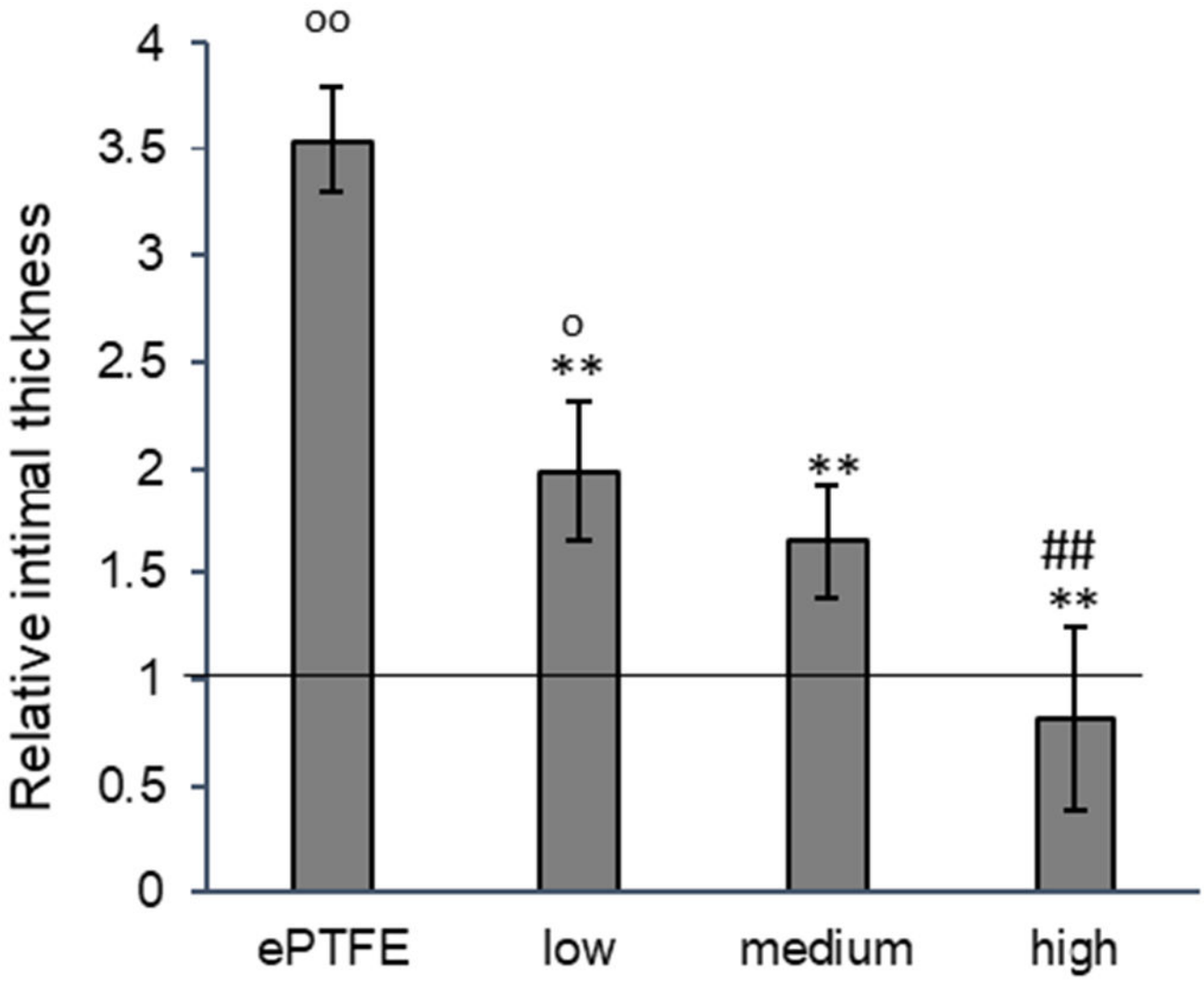

Figure 8:

Quantification of the intima:media ratio as assessed by disruption of the laminar structure of elastic fibers. The black line denotes sham control. Statistical differences as determined by ANOVA with a post-hoc Tukey's test are represented by the following: oo = different from sham, $p < 0.05$; o = different from sham, $p < 0.10$; ** = different from ePTFE, $p < 0.05$; ## = different from low compliance, $p < 0.05$.

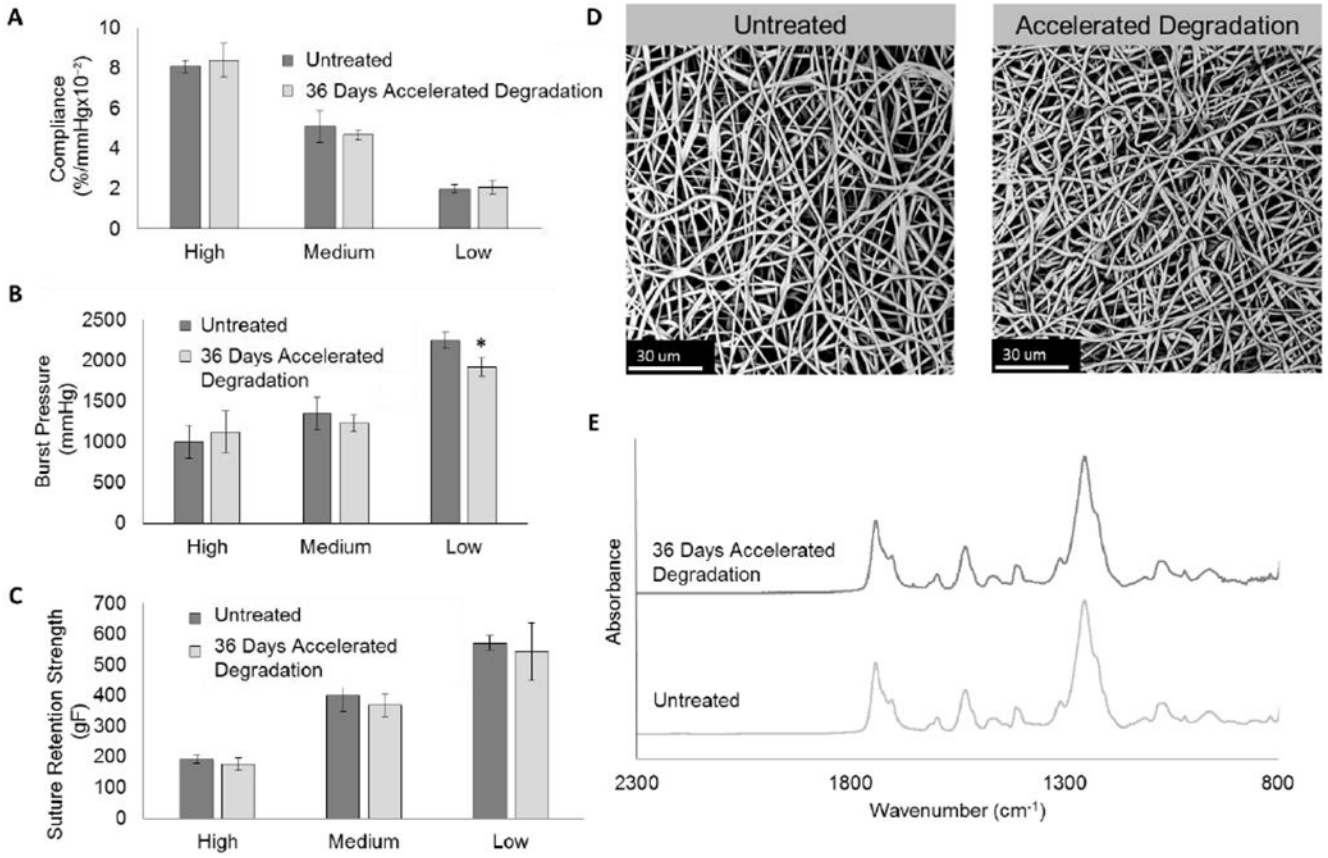

Figure 9:

The effects of accelerated oxidative degradation for 36 days in 0.1M $CoCl_2$ in 20% H_2O_2 on the compliance (A), burst pressure (B), and suture retention strength (C) of the low, medium, and high compliance multilayered vascular grafts. The effects of oxidative degradation on fiber morphology determined by SEM (D) and surface chemistry determined by ATR (E). Data is represented as average ± standard deviation for an n=4. Statistical significance is shown by * to show a difference between untreated and treated groups with $p<0.05$.